# Rotor flux and EEMF observer for interior permanent magnet synchronous machine

Deepak VYAS*, Marcin MORAWIEC[ID], and DANIEL WACHOWIAK[ID]

Department of Electric Drives and Energy Conversion, Faculty of Electrical and Control Engineering and EkoTech Center, Gdańsk University of Technology, ul. Narutowicza 11/12, 80-233 Gdańsk, Poland

**Abstract.** In recent years, the use of the interior permanent magnet synchronous machine (IPMSM) in various applications has grown significantly due to numerous benefits. Sensors are used to achieve high efficiency and good dynamic response in IPMSM drives but due to their high cost and reduced overall size of the system, sensorless control techniques are preferred. Non-sinusoidal distribution of rotor flux and slot harmonics are present in the considered IPMSM. In this article, these problems are considered control system disturbances. With the above-mentioned problems, the classical observer structure based on (d-q) fails to estimate at low-speed ranges. This article proposes an observer structure based on a rotor flux vector in ($\alpha$-$\beta$) stationary reference frame, which works using the adaptive control law to estimate speed and position, and a non-adaptive EEMF-based observer to estimate speed and position. Moreover, a comparative analysis between both observer structures at different speed ranges is also considered in this article. The effectiveness of the observer structure is validated by simulation tests and experimental tests using the sensorless control system with a field-oriented control scheme for a 3.5 kW IPMSM drive system.

**Keywords:** field oriented-control; interior permanent magnet synchronous machine; model-based method; sensorless control; saliency-based techniques.

## 1. INTRODUCTION

Permanent magnet synchronous motors (PMSM) offer high torque density, fast dynamic response, high reliability, and good power factor. Due to the above advantages, it became popular in industrial applications, including traction, domestic appliances, and seabed mining. Surface-mounted permanent magnet synchronous motors (SPMSM), where magnets are mounted on the surface of the rotor, and interior permanent magnet synchronous motors, where magnets are buried inside the rotor core, are two main types of PMSM. IPMSM provides reluctance torque and better field weakening control, which gives the edge compared to SPMSM. This article considers IPMSM throughout the discussion of sensorless control methods. Sensorless control offers various advantages, such as reduced cost and size, and improves the reliability of the IPMSM drive. Researchers across the globe have been making excellent efforts to develop novel sensorless control techniques for a wide speed of operation of IPMSM drives [1–7].

For sensorless control of IPMSM, two main approaches of sensorless control schemes are the model-based and saliency-based methods. Generally, the model-based method works well at medium and high-speed ranges, while the saliency-based method performs well at zero and low-speed ranges. The model-based method can be implemented with the help of electromotive force (EMF), and saliency-based estimators require signal injection to obtain information on the rotor position. The main concept behind the saliency-based approach is that machine winding inductances are the function of the rotor position due to its saliency, and with the variation in inductance, rotor position can be obtained. Recently, methods based on artificial intelligence have also been introduced to apply sensorless control [1,8].

Predictive current control based on internal model control observer for PMSM proposed in [9] works well in terms of feasibility, robustness, and control, but suffers from internal disturbance. Navaneethan *et al.* proposed a Lyapunov stability-based sliding mode observer to estimate speed and current; however, the performance of the proposed observer was not discussed at zero speed range [10]. In [11], a rotor flux vector-based adaptive observer structure on an alpha-beta reference frame was proposed to estimate the speed and position of the IPMSM. J. Choi *et al.* proposed a regression model considering the parameter estimator and flux observer. However, the accuracy problem can be seen in the observer performance at low speeds [12]. A cascade design approach is used to prepare adaptive full-order observers for IPMSM. The proposed technique reduced the number of gains in the observer structure. The proposed control strategy becomes stagnant during the standstill position and unobservable during the low-speed range [13].

A novel frequency adaptive second-order disturbance observer is presented in [14]. The observer structure works well for different speed ranges, but some inaccuracy can be observed near zero speed ranges. Similarly, a third-order super-twisting and nonlinear extended state observer for IPMSM are discussed in [14], and [15], respectively. These observer structures also suffer at low-speed ranges. In the IPMSM drive, model reference adaptive systems (MRAS), adaptive filters, sliding mode

*e-mail: deevyas@pg.edu.pl

D. Vyas, M. Morawiec, and D. Wachowiak

observers, and extended state observers are popular closed-loop observer techniques that can be implemented. Alternative observer structures for the sensorless control of IPMSM are proposed in [17–23]. However, implementing this method is sometimes not straightforward in engineering practice due to the complex sensorless control structure.

In this article, we propose a rotor flux vector-based adaptive observer and the extended EMF (EEMF) based non-adaptive observer for IPMSM drive to estimate the value of speed and position. The IPMSM presented in the paper has spatial harmonics and has the problem of non-sinusoidal EMF. Due to this non-symmetry of the machine, the mathematical model of the proposed observer structures for adaptive based on rotor flux and non-adaptive based on extended EMF is in the form ($\alpha$-$\beta$) reference frame and stabilized using the Lyapunov criteria. Compared to the (d-q) reference frame, observer structure in the ($\alpha$-$\beta$) reference frame is more robust during the disturbances as state variables are not required to transform through estimated rotor position to the (d-q) reference frame. In the adaptive observer, rotor speed is estimated using conventional adaptive law, which reduces the order of the observer structure, and angular position is calculated by integrating the value of rotor speed [24]. When an angular position is estimated through integration, the stability question arises because the integrator is in the open loop. Additional feedback laws are implemented to overcome the stability problem and improve the observer's work. The proposed stabilizing functions are non-continuous or constant, specifically during low-speed range or at standstill operation of IPMSM. The added extra feedback laws for rotor speed and position satisfy the persistent excitation condition and ensure the stability of the sensorless control, especially during low speed with torque injection [25]. In non-adaptive observers, speed is estimated using the dependence of extended EMF and rotor flux, and angular position is calculated using the angle observed between induced EMF. The motivation of this work is to develop and apply comparative analysis between adaptive and non-adaptive observer structures. The main contribution of this article can be summarized as follows:

1. Considering slot harmonics in the IPMSM, develop an observer structure that works well during all speed ranges. The observer structure is in the form ($\alpha$-$\beta$) reference frame. It is assumed that slot harmonics are compensated in the control system.
2. Provide a comparative analysis of the performance of adaptive rotor flux vector-based observer and non-adaptive extended EMF-based observer.
3. Position estimation is improved due to the proposed stabilizing function, especially for low-speed ranges.

The proposed approaches are validated through theoretical, simulation, and experimental investigations on 3.5 kW IPMSM with non-sinusoidal back-EMF distribution.

## 2. MATHEMATICAL MODEL OF IPMSM

The mathematical model of the IPMSM can be prepared in the different reference frames. The equivalent circuit of IPMSM in d-q reference frame [25–27] is shown in Fig. 1.
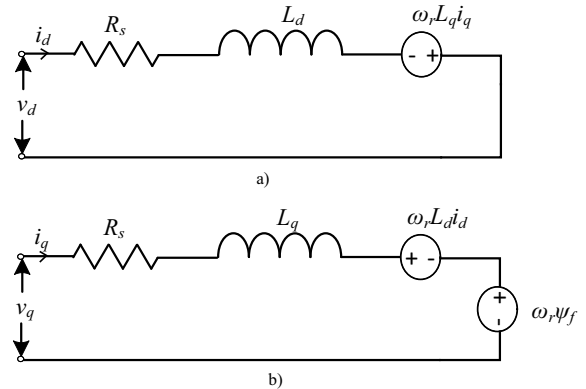


**Fig. 1.** Dynamic equivalent circuit of IPMSM in d-q reference frame a) d-axis equivalent circuit; b) q-axis equivalent circuit

Using the reference frame transformation dynamical model of the IPMSM based on stator currents in the ($\alpha$-$\beta$) reference frame is well-known in the literature [25–27]:

$$\frac{\mathrm{d}i_{s\alpha}}{\mathrm{d}\tau} = \frac{\omega_r}{L_d}\lambda_\beta + (-R_s i_{s\alpha} + u_{s\alpha})L_1 + (-R_s i_{s\beta} + u_{s\beta})L_3, \quad (1)$$

$$\frac{\mathrm{d}i_{s\beta}}{\mathrm{d}\tau} = -\frac{\omega_r}{L_d}\lambda_\alpha + (-R_s i_{s\alpha} + u_{s\alpha})L_3 + (-R_s i_{s\beta} + u_{s\beta})L_4, \quad (2)$$

$$\frac{\mathrm{d}\omega_r}{\mathrm{d}\tau} = \frac{1}{J}(\psi_{f\alpha}i_{s\beta} - \psi_{f\beta}i_{s\alpha} + (L_d - L_q)i_{s\alpha}i_{s\beta} - T_L), \quad (3)$$

$$\frac{\mathrm{d}\theta_r}{\mathrm{d}\tau} = \omega_r, \quad (4)$$

$$\lambda_\alpha = \frac{L_d}{L_q}\psi_{f\alpha} - \left(1 - \frac{L_d}{L_q}\right)(L_0 i_{\alpha 2} + L_2 i_{s\alpha}), \quad (5)$$

$$\lambda_\beta = \frac{L_d}{L_q}\psi_{f\beta} + \left(1 - \frac{L_d}{L_q}\right)(L_0 i_{\beta 2} - L_2 i_{s\beta}). \quad (6)$$

The dynamical model of IPMSM considering EEMF can be modeled by state space equation in stationary reference frame as given by:

$$\frac{\mathrm{d}i_{s\alpha}}{\mathrm{d}\tau} = \frac{1}{L_q}e_\beta + \omega_r\lambda_\beta + (-R_s i_{s\alpha} + u_{s\alpha})L_1$$
$$+ (-R_s i_{s\beta} + u_{s\beta})L_3, \quad (7)$$

$$\frac{\mathrm{d}i_{s\beta}}{\mathrm{d}\tau} = -\frac{1}{L_q}e_\alpha + \omega_r\lambda_\alpha + (-R_s i_{s\alpha} + u_{s\alpha})L_3$$
$$+ (-R_s i_{s\beta} + u_{s\beta})L_4, \quad (8)$$

$$\frac{\mathrm{d}e_\alpha}{\mathrm{d}\tau} = \frac{\mathrm{d}\omega_r}{\mathrm{d}\tau}\psi_{f\alpha} - \omega_r e_\beta, \quad (9)$$

$$\frac{\mathrm{d}e_\beta}{\mathrm{d}\tau} = \frac{\mathrm{d}\omega_r}{\mathrm{d}\tau}\psi_{f\beta} + \omega_r e_\alpha, \quad (10)$$

where

$$\lambda_\alpha = \left(\frac{1}{L_d} - \frac{1}{L_q}\right)\left(\frac{1}{L_d}L_0 i_{\alpha 2} + \frac{1}{L_d}L_2 i_{s\alpha}\right), \quad (11)$$

$$\lambda_\beta = \left(\frac{1}{L_d} - \frac{1}{L_q}\right)\left(\frac{1}{L_d}L_0 i_{\beta 2} - \frac{1}{L_d}L_2 i_{s\beta}\right), \quad (12)$$

where $R_s$ is stator resistance; $L_d$ and $L_q$ are winding inductances; $J$ is inertia; $T_L$ and $T_e$ is load and electromagnetic torque, respectively; $u_{s\alpha,\beta}$, $i_{s\alpha,\beta}$ and $\psi_{f\alpha,\beta}$ are the vector components of stator voltage current and permanent magnet flux, respectively; $\omega_r$ and $\theta_r$ rotor angular speed and position of the rotor; $\lambda_\alpha$ and $\lambda_\beta$ are defined as rotor flux vector components. The parameters $L_0$, $L_2$ and functions $L_1$, $L_3$, $L_4$, and the park transformation of stator current are defined in Section 3.1. In the given model $e_{\alpha,\beta}$ are the vector components of EMF. It is assumed that the parameters of the machine are considered unchanging in time. Sinusoidal and non-sinusoidal EMF distribution with additional spatial harmonics occurs in the IPMSM.

In this article, the effect of non-sinusoidal distribution in the IPMSM is considered, and the waveform of non-sinusoidal EMF can be seen in Fig. 2. The total number of slots is 36, and the eighteenth harmonics is dominant. In this article, the harmonics are not compensated using an extended control system. These disturbances are considered in the observer structure to achieve desirable sensorless control of the IPMSM. Due to these disturbances, the design procedure of the observer becomes slightly complex. The next section presents and explains the observer structure for both cases in detail.
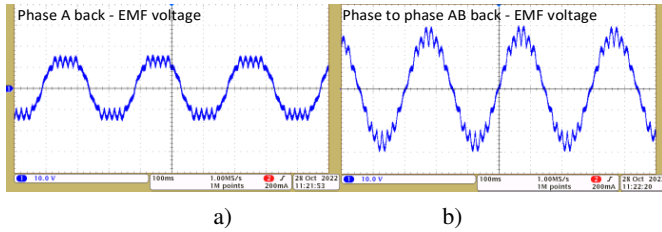


**Fig. 2.** Dynamic equivalent circuit of IPMSM in d-q reference frame
a) d-axis equivalent circuit; b) q-axis equivalent circuit

## 3. SPEED AND POSITION OBSERVER STRUCTURE

### 3.1. Adaptive observer structure

Firstly, the adaptive observer structure based on the rotor flux vector will be presented, followed by the non-adaptive speed and position observer structure. This paper considers a model based on $(\alpha\text{-}\beta)$ reference frame connected to the stator and compares the performance with the EEMF non-adaptive observer structure. The observer model contains $L_1$, $L_3$ and $L_4$ introduced to equations (1) and (2), which are the rotor position functions, making this observer structure non-symmetrical. The observer structure can be designed using the mathematical model of IPMSM equations (1)–(4). The symbols such as "$\wedge$" and "$\sim$" are used for estimated and error values:

$$\frac{d\hat{i}_{s\alpha}}{d\tau} = \frac{\hat{\omega}_r}{L_d}\hat{\lambda}_\beta + \left(-R_s\hat{i}_{s\alpha} + u_{s\alpha}\right)L_1$$
$$+ \left(-R_s\hat{i}_{s\beta} + u_{s\beta}\right)L_3 + v_\alpha, \tag{13}$$

$$\frac{d\hat{i}_{s\beta}}{d\tau} = -\frac{\hat{\omega}_r}{L_d}\hat{\lambda}_\alpha + \left(-R_s\hat{i}_{s\alpha} + u_{s\alpha}\right)L_3$$
$$+ \left(-R_s\hat{i}_{s\beta} + u_{s\beta}\right)L_4 + v_\beta, \tag{14}$$

$$\frac{d\hat{\theta}_r}{d\tau} = \hat{\omega}_r + v_\theta, \tag{15}$$

$$\hat{\lambda}_\alpha = \frac{L_d}{L_q}\psi_{f\alpha} - \left(1 - \frac{L_d}{L_q}\right)\left(L_0\hat{i}_{\alpha2} + L_2\hat{i}_{s\alpha}\right), \tag{16}$$

$$\hat{\lambda}_\beta = \frac{L_d}{L_q}\psi_{f\beta} + \left(1 - \frac{L_d}{L_q}\right)\left(L_0\hat{i}_{\beta2} - L_2\hat{i}_{s\beta}\right). \tag{17}$$

It can be seen that in equations (13)–(15), stabilizing functions are introduced $v_{\alpha,\beta}$, and $v_\theta$. The final form of stabilizing function can be derived with the help of Lyapunov stability criteria. In the observer model, $u_{s\alpha,\beta}$ is the stator voltage vector component considered the known value. The component of rotor flux can be estimated using equations (16) and (17). It is assumed that the functions $L_1$, $L_2$, $L_3$, $L_4$, $i_{s\alpha2}$, $i_{s\beta2}$, $\psi_{f\alpha}$, and $\psi_{f\beta}$ defined in observer structure from (13) to (17) are calculated using the estimated value of rotor position and stator current vector components:

$$L_0 = 0.5\left(L_d + L_q\right), \qquad L_2 = 0.5\left(L_d - L_q\right), \tag{18}$$

$$L_1 = L_d^{-1}\cos^2\hat{\theta}_r + L_q^{-1}\sin^2\hat{\theta}_r, \tag{19}$$

$$L_3 = 0.5\left(L_d^{-1} - L_q^{-1}\right)\sin(2\hat{\theta}_r), \tag{20}$$

$$L_4 = L_d^{-1}\sin^2\hat{\theta}_r + L_q^{-1}\cos^2\hat{\theta}_r, \tag{21}$$

$$\hat{i}_{s\alpha2} = \hat{i}_{s\alpha}\cos(2\hat{\theta}_r) + \hat{i}_{s\beta}\sin(2\hat{\theta}_r), \tag{22}$$

$$\hat{i}_{s\beta2} = -\hat{i}_{s\alpha}\sin(2\hat{\theta}_r) + \hat{i}_{s\beta}\cos(2\hat{\theta}_r), \tag{23}$$

$$\hat{\psi}_{f\alpha} = \psi_f\cos\hat{\theta}_r, \tag{24}$$

$$\hat{\psi}_{f\beta} = \psi_f\sin\hat{\theta}_r. \tag{25}$$

The next step is to stabilize the observer structure using the Lyapunov stability theorem. A stabilizing function in the observer structure equations (13)–(15) will be formed using Lyapunov stability criteria. As per the Lyapunov stability criteria, a positively determined candidate function should be defined first. The chosen quadratic Lyapunov function has the following form:

$$V = 0.5\left(\left(\tilde{i}_{s\alpha}^2 + \tilde{i}_{s\beta}^2\right) + \tilde{\theta}_r^2\right). \tag{26}$$

The error between estimated and measured parameters can be calculated using equation (27)

$$\tilde{i}_{s\alpha,\beta} = \hat{i}_{s\alpha,\beta} - i_{s\alpha,\beta}, \quad \tilde{\omega}_r = \hat{\omega}_r - \omega_r, \quad \tilde{\theta}_r = \hat{\theta}_r - \theta_r. \tag{27}$$

The derivative of the defined Lyapunov function should be negatively determined. After substituting appropriate terms in equa-

*Bull. Pol. Acad. Sci. Tech. Sci.*, vol. 72, no. 4, p. e150327, 2024

3

tion (26) yields

$$\dot{V} = \tilde{i}_{s\alpha} \left( \begin{array}{c} \frac{1}{L_d} (\hat{\omega}_r (\hat{\lambda}_\beta - \tilde{\lambda}_\beta) - \tilde{\omega}_r (\lambda_\beta - \tilde{\lambda}_\beta) \\ -R_s (\tilde{i}_{s\alpha} L_1 + \tilde{i}_{s\beta} L_3) + v_\alpha \end{array} \right)$$
$$+ \tilde{i}_{s\beta} \left( \begin{array}{c} -\frac{1}{L_d} (\hat{\omega}_r (\hat{\lambda}_\alpha - \tilde{\lambda}_\alpha) - \tilde{\omega}_r (\lambda_\alpha - \tilde{\lambda}_\alpha) \\ -R_s (\tilde{i}_{s\alpha} L_3 + \tilde{i}_{s\beta} L_4) + v_\beta \end{array} \right)$$
$$+ \tilde{\theta}_r (\tilde{\omega}_r + v_\theta) \leq 0. \tag{28}$$

The given observer structure is asymptotically stable if obtained stabilizing functions have the following form and $c_\alpha$, $c_\lambda$, $c_\theta > 0$ are introduced to the stabilizing functions in equations (29), (30), and (31)

$$v_\alpha = -c_a R_s L_1 \tilde{i}_{s\alpha} + c_\lambda \frac{1}{L_d} \hat{\omega}_r \hat{\lambda}_\beta \tilde{i}_{s\alpha}, \tag{29}$$

$$v_\beta = -c_a R_s L_4 \tilde{i}_{s\beta} - c_\lambda \frac{1}{L_d} \hat{\omega}_r \hat{\lambda}_\alpha \tilde{i}_{s\beta}, \tag{30}$$

$$v_\theta = -c_\theta \tilde{\theta}_r. \tag{31}$$

The positively defined Lyapunov function can be extended to obtain an estimated speed. The extended positively defined Lyapunov function and its derivative are given below, respectively:

$$V_1 = \frac{1}{\gamma} \tilde{\omega}_r^2, \tag{32}$$

$$\dot{V}_1 = \tilde{\omega}_r \frac{1}{L_d} \left( -\hat{\lambda}_\beta \tilde{i}_{s\alpha} + \hat{\lambda}_\alpha \tilde{i}_{s\beta} + \frac{1}{\gamma} \dot{\hat{\omega}}_r \right) \leq 0. \tag{33}$$

From equation (33), by using an adaptive mechanism, the value of rotor speed can be estimated directly

$$\dot{\hat{\omega}}_r = \gamma \frac{1}{L_d} (\hat{\lambda}_\beta \tilde{i}_{s\alpha} - \hat{\lambda}_\alpha \tilde{i}_{s\beta}), \quad \gamma > 0 \quad \& \quad \dot{\hat{\omega}}_r \approx \dot{\omega}_r. \tag{34}$$

Estimation errors will converge to zero in finite time $t > t_1$ since the machine model remains in the operation domain D. It can be represented as

$$c_{\alpha 1} = \max \{\tilde{i}_{s\alpha} R_s L_1\} + \delta_1, \tag{35}$$

$$c_{\alpha 2} = \max \{\tilde{i}_{s\beta} R_s L_4\} + \delta_2, \tag{36}$$

$$c_\theta = \max \{\tilde{\theta}_r \tilde{\omega}_r^{-1}\} + \delta_\theta, \tag{37}$$

With $\delta_1$, $\delta_2$, $\delta_\theta > 0$ and for $\tilde{i}_{s\alpha,\beta} \leq \varepsilon_1$, $\tilde{\theta}_r \leq \varepsilon_2$, $\tilde{\omega}_r \leq \varepsilon_3$ and $\varepsilon_{1,2,3} \ll 1$ are sufficient small reals, and the derived derivative of the Lyapunov function takes the following form:

$$\dot{V} = -\delta_\alpha |\tilde{i}_{s\alpha}| - \delta_\beta |\tilde{i}_{s\beta}| - \delta_\theta |\tilde{\theta}_r| \leq -\mu \sqrt{V}, \tag{38}$$

where $\mu = \min(\sqrt{2\delta_\alpha} \sqrt{2\delta_\beta} \sqrt{2\delta_\theta})$ and $\delta_\alpha = \delta_1 + \delta_2$. The defined condition in equation (38) applies to the convergence of vector values of $\hat{i}_s$ to $i_s$ and $\vec{\hat{\lambda}}$ to $\lambda$. Hence $\hat{\theta}_r$, it tends to have real value $\theta_r$ in finite time, denoted as $t_2$. For $(\hat{\lambda}_\beta \tilde{i}_{s\alpha} \hat{\lambda}_\alpha \tilde{i}_{s\beta}) \neq 0$ and

$\gamma > 0$, the estimated angular speed of the rotor form equation (34) converges exponentially to its real value $\omega_r$. Assuming that $c_\alpha = c_{\alpha 1} = c_{\alpha 2}$, the value of $c_\alpha$ can be determined from equation (39) and $c_\lambda$ can be calculated by assuming $c_\alpha = 1$ and $|\hat{\omega}_r|(\hat{\lambda}_\alpha^2 + \hat{\lambda}_\beta^2)$ from equation (40)

$$c_\alpha = \max \left\{ R_s \tilde{i}_{sa} \sqrt{L_1^2 + L_4^2} \right\}, \tag{39}$$

$$0 \leq c_\lambda \leq \frac{R_s L_1 \hat{\lambda}_\beta - R_s L_4 \hat{\lambda}_\alpha}{L_d^{-1} |\hat{\omega}_r| \left(\hat{\lambda}_a^2 + \hat{\lambda}_\beta^2\right)}. \tag{40}$$

It can be seen that in equation (31), an angular position error exists. However, the angular position error cannot be implemented as in a sensorless control system angular position and speed are not measured. Hence, instead $\tilde{\theta}_r$, the approximated value of this error $\tilde{\theta}_\lambda$, can be used, and equation (31) can be rewritten as

$$v_\theta = -c_\theta \tilde{\theta}_\lambda. \tag{41}$$

Vectors rotate at synchronous speed of the flux vector of the permanent magnets, which is equivalent to the rotor angular speed. The position of the rotor is the same as the position of the flux vector of permanent magnets. Hence, the position error between the rotor flux vector can be estimated firstly from equations (16) and (17) and secondly from equations (5) and (6). Vector $\lambda_{\alpha,\beta}$ can be calculated using equations (5) and (6), in which it can be assumed that $\theta_r \approx \hat{\theta}_r$, the measured currents are used, and $(\lambda_\alpha \hat{\lambda}_\alpha + \lambda_\beta \hat{\lambda}_\beta)$. $\tilde{\theta}_\lambda$ can be seen in Fig. 3. The value $\tilde{\theta}_\lambda$ is close to 0, and after amplifying, the value can be $\tilde{\theta}_r \approx \tilde{\theta}_\lambda$. Value $\tilde{\theta}_\lambda$ can be projected by

$$\tilde{\theta}_\lambda = \tan^{-1}(\varphi), \tag{42}$$

$$\varphi = \frac{(\lambda_\alpha \hat{\lambda}_\beta - \lambda_\beta \hat{\lambda}_\alpha)}{(\lambda_\alpha \hat{\lambda}_\alpha + \hat{\lambda}_\beta \lambda_\beta)}, \tag{43}$$

$$\tilde{\theta}_\lambda = \begin{cases} \tilde{\theta}_\lambda - \pi/2, & \varphi \geq 0 \\ \tilde{\theta}_\lambda + \pi/2, & \varphi < 0 \end{cases}. \tag{44}$$
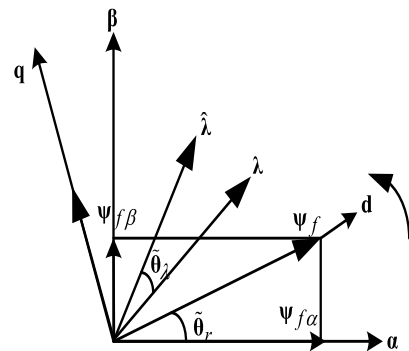


**Fig. 3.** The space vector representation of IPMSM in the $\alpha$-$\beta$ plane

From equation (34), the estimated value of rotor speed can be obtained. Stator current deviation and the vector components

4

*Bull. Pol. Acad. Sci. Tech. Sci.*, vol. 72, no. 4, p. e150327, 2024

of rotor flux are used to calculate the estimated speed. It can be seen that it is a cross-product of these vectors. The mutual position of these vectors changes at different working instances of the IPMSM. The scalar product of these vectors is zero if it is assumed that these vectors are perpendicular. In practice, the scalar product cannot become zero due to the tuning gains of the observer – equations (38) and (40). Moreover, errors in the estimation of the speed will be dependent on the scalar product of these two vectors. Hence, an improved estimation law is proposed in the article to enhance the quality of estimation of the observer structure. The improved estimation is based on the cross and scalar product of the rotor flux and stator current errors. The improved estimation law is as follows, and the value of $|s_\omega| \le \varepsilon_\omega$ is bounded

$$\dot{\hat{\omega}}_r = \gamma \frac{1}{L_d} \left( \hat{\lambda}_\beta \tilde{i}_{s\alpha} - \hat{\lambda}_\alpha \tilde{i}_{s\beta} - k_c s_\omega \right), \tag{45}$$

$$s_\omega = \left( \hat{\lambda}_\alpha \tilde{i}_{s\alpha} + \hat{\lambda}_\beta \tilde{i}_{s\beta} \right). \tag{46}$$

Here, gain $k_c$ is essential when the machine passes through zero speed. The given position and speed observer system are observable for rotor speed $\omega_r \ne 0$ or satisfy the four conditions.

### 3.2. Non-adaptive EEMF observer structure

The non-adaptive approach to estimate speed and position can be prepared from the observer structure based on the mathematical model equations (7)–(10). It is important to mention the observability of the system before proposing an observer structure. The observability rank is 4 and the determinant of the observability matrix is nonsingular which satisfies the criteria of observability. Hence, the system is observable [25–27]. The form of the observer structure is given below:

$$\frac{\mathrm{d}\hat{i}_{s\alpha}}{\mathrm{d}\tau} = \frac{1}{L_q}\hat{e}_\beta + \hat{\omega}_r \hat{\lambda}_\beta + (-R_s \hat{i}_{s\alpha} + u_{s\alpha})L_1$$
$$+ (-R_s \hat{i}_{s\beta} + u_{s\beta})L_3 + v_\alpha, \tag{47}$$

$$\frac{\mathrm{d}\hat{i}_{s\beta}}{\mathrm{d}\tau} = -\frac{1}{L_q}\hat{e}_\alpha + \hat{\omega}_r \hat{\lambda}_\alpha + (-R_s \hat{i}_{s\alpha} + u_{s\alpha})L_3$$
$$+ (-R_s \hat{i}_{s\beta} + u_{s\beta})L_4 + v_\beta, \tag{48}$$

$$\frac{\mathrm{d}\hat{e}_\alpha}{\mathrm{d}\tau} = \frac{\mathrm{d}\hat{\omega}_r}{\mathrm{d}\tau}\psi_{f\alpha} - \hat{\omega}_r \hat{e}_\beta + v_{e\alpha}, \tag{49}$$

$$\frac{\mathrm{d}\hat{e}_\beta}{\mathrm{d}\tau} = \frac{\mathrm{d}\hat{\omega}_r}{\mathrm{d}\tau}\psi_{f\beta} + \hat{\omega}_r \hat{e}_\alpha + v_{e\beta}, \tag{50}$$

$$\hat{\lambda}_\alpha = \left( \frac{1}{L_d} - \frac{1}{L_q} \right)\left( \frac{1}{L_d}L_0 \hat{i}_{\alpha 2} + \frac{1}{L_d}L_2 \hat{i}_{s\alpha} \right), \tag{51}$$

$$\hat{\lambda}_\beta = \left( \frac{1}{L_d} - \frac{1}{L_q} \right)\left( \frac{1}{L_d}L_0 \hat{i}_{\beta 2} - \frac{1}{L_d}L_2 \hat{i}_{s\beta} \right). \tag{52}$$

The newly added input variables in the observer structures are $v_\alpha$, $v_\beta$, $v_{e\alpha}$, and $v_{e\beta}$ are considered stabilizing functions. With the help of this stabilizing function, the observer structure can

converge to the real value of the machine. In equations (49) and (50), the derivative of rotor speed can be approximated, considering the $d\hat{\omega}_r/d\tau \approx \Delta\hat{\omega}_r/\Delta\tau$. Moreover, this term does not impact accuracy while estimating rotor speed and position. As used in earlier observer structures, the Lyapunov theorem will significantly help define the stabilizing function. Estimation error can be defined as:

$$\tilde{i}_{s\alpha,\beta} = \hat{i}_{s\alpha,\beta} - i_{s\alpha,\beta}, \quad \tilde{e}_{\alpha,\beta} = \hat{e}_{\alpha,\beta} - e_{\alpha,\beta},$$
$$\tilde{\omega}_r = \hat{\omega}_r - \omega_r, \qquad \tilde{\theta}_r = \hat{\theta}_r - \theta_r. \tag{53}$$

As per the Lyapunov function, a first positively determined function is defined, and the function derivative should be negatively determined $\dot{V} \le 0$, which can be seen in equations (54) and (55), respectively:

$$V = \frac{1}{2}\left( \tilde{i}_{s\alpha}^2 + \tilde{i}_{s\beta}^2 \right), \tag{54}$$

$$\dot{V} = \tilde{i}_{s\alpha}\left( \begin{array}{c} \frac{1}{L_q}\tilde{e}_\beta + (\hat{\omega}_r(\hat{\lambda}_\beta - \tilde{\lambda}_\beta) - \tilde{\omega}_r(\lambda_\beta - \tilde{\lambda}_\beta) + \\ (-R_s\tilde{i}_{s\alpha} + u_{s\alpha})L_1 + (-R_s\tilde{i}_{s\beta} + u_{s\beta})L_3 + v_\alpha \end{array} \right)$$
$$+ \tilde{i}_{s\beta}\left( \begin{array}{c} -\frac{1}{L_q}\tilde{e}_\alpha + (\hat{\omega}_r(\hat{\lambda}_\alpha - \tilde{\lambda}_\alpha) - \tilde{\omega}_r(\lambda_\alpha - \tilde{\lambda}_\alpha) + \\ (-R_s\tilde{i}_{s\alpha} + u_{s\alpha})L_3 + (-R_s\tilde{i}_{s\beta} + u_{s\beta})L_4 + v_\beta \end{array} \right). \tag{55}$$

The proposed observer structure is asymptotic and stable if the stabilizing function has the following form: Gains $c_\alpha$, $c_{e\alpha}$, and $c_{e\beta}$ are > 0.

$$v_\alpha = -c_\alpha R_s L_1 \tilde{i}_{s\alpha}, \tag{56}$$

$$v_\beta = -c_\alpha R_s L_4 \tilde{i}_{s\beta}, \tag{57}$$

$$v_{e\alpha} = c_{e\alpha}\frac{1}{L_q}\tilde{i}_{s\beta}, \tag{58}$$

$$v_{e\beta} = -c_{e\beta}\frac{1}{L_q}\tilde{i}_{s\alpha}. \tag{59}$$

The estimated angular speed and position value can be determined from the dependence of EEMF and permanent magnet flux components [28]. It is worth mentioning that $\hat{\psi}_{f\alpha}^2 + \hat{\psi}_{f\beta}^2 \ne 0$ flux components tend to have real values in finite time, and estimated speed converges exponentially to their real value

$$\hat{\omega}_r = \frac{\hat{e}_\alpha \hat{\psi}_{f\alpha} + \hat{e}_\beta \hat{\psi}_{f\beta}}{\hat{\psi}_{f\alpha}^2 + \hat{\psi}_{f\beta}^2}, \tag{60}$$

$$\hat{\theta}_r = a\tan\left( \hat{e}_\beta, \hat{e}_\alpha \right). \tag{61}$$

## 4. SENSORLESS CONTROL SCHEME

In this article, a classical control scheme known as field-oriented control is employed. The block diagram of the control scheme is shown in Fig. 4. As shown in Fig. 4, the Clarke transformation is used to convert three-phase currents ($i_{sa}$, $i_{sb}$, $i_{sc}$) into two-phase ($i_{s\alpha}$, $i_{s\beta}$) reference frame for the observer structure implementation.

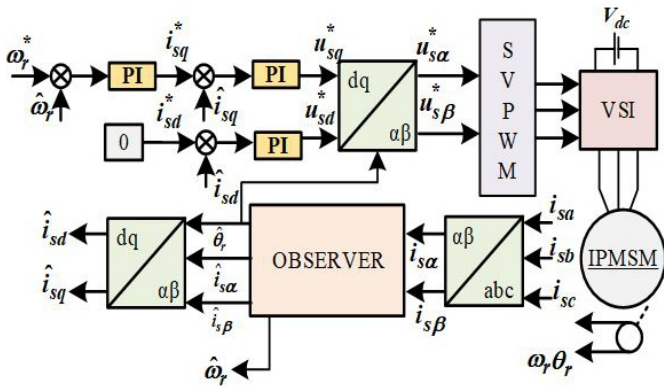*Bull. Pol. Acad. Sci. Tech. Sci.*, vol. 72, no. 4, p. e150327, 2024

5

**Fig. 4.** The sensorless control scheme of the IPMSM machine

Estimated parameters such as currents, speed, and angular position are defined using the symbol "^". Estimated currents from the observer are transformed to $(i_{sd}, i_{sq})$ d-q reference frame using estimated angular position $(\theta_r)$ to implement field-oriented control (FOC). Controllers in field-oriented control compare ref-

erence values of speed $(\omega_r^*)$, currents $(i_{sd}^*, i_{sq}^*)$, and estimated values of speed $(\hat{\omega}_r)$ and currents $(\hat{i}_{sd}, \hat{i}_{sq})$, and based on the error signal, they generate the control signal for the IPMSM drive. In this article, the classical FOC scheme considering $i_{sd}^* = 0$ is implemented.

Figures 5a and 5b show simulation results for adaptive and non-adaptive EEMF-based observer structures. Reference values $\omega_r^* = 0.0$ to 0.8 p.u. and 0.8 to $-0.8$ p.u., $T_L = 0.3$ p.u. are considered for adaptive observer structure, and $\omega_r^* = 0.0$ to 0.8 and 0.8 to $-0.8$, $T_L = 0.1$ are considered for non-adaptive observer structure. Simulation results show that the estimated speed $\hat{\omega}_r$ and position $\hat{\theta}_r$ follow the measured value of respective parameters. During zero-crossing states, speed $\tilde{\omega}_r$ and position errors $\tilde{\theta}_r$ are higher in non-adaptive EEMF-based observers. Estimated currents $\hat{i}_{sd}, \hat{i}_{sq}$ for respective observer structures are depicted in Fig. 5.

$c_\alpha = 0.6$, $c_\lambda = 0.1$, $c_\theta = 0.1$, and $k_c = 0.1$ are the gains of the stabilizing functions used in adaptive observer structure. Tuning gains of non-adaptive EEMF-based observer structure are as $c_\alpha = 3.1$, $c_{e\alpha} = 0.9$, $c_{e\beta} = 0.9$. Experimental results are discussed in detail in the next section.
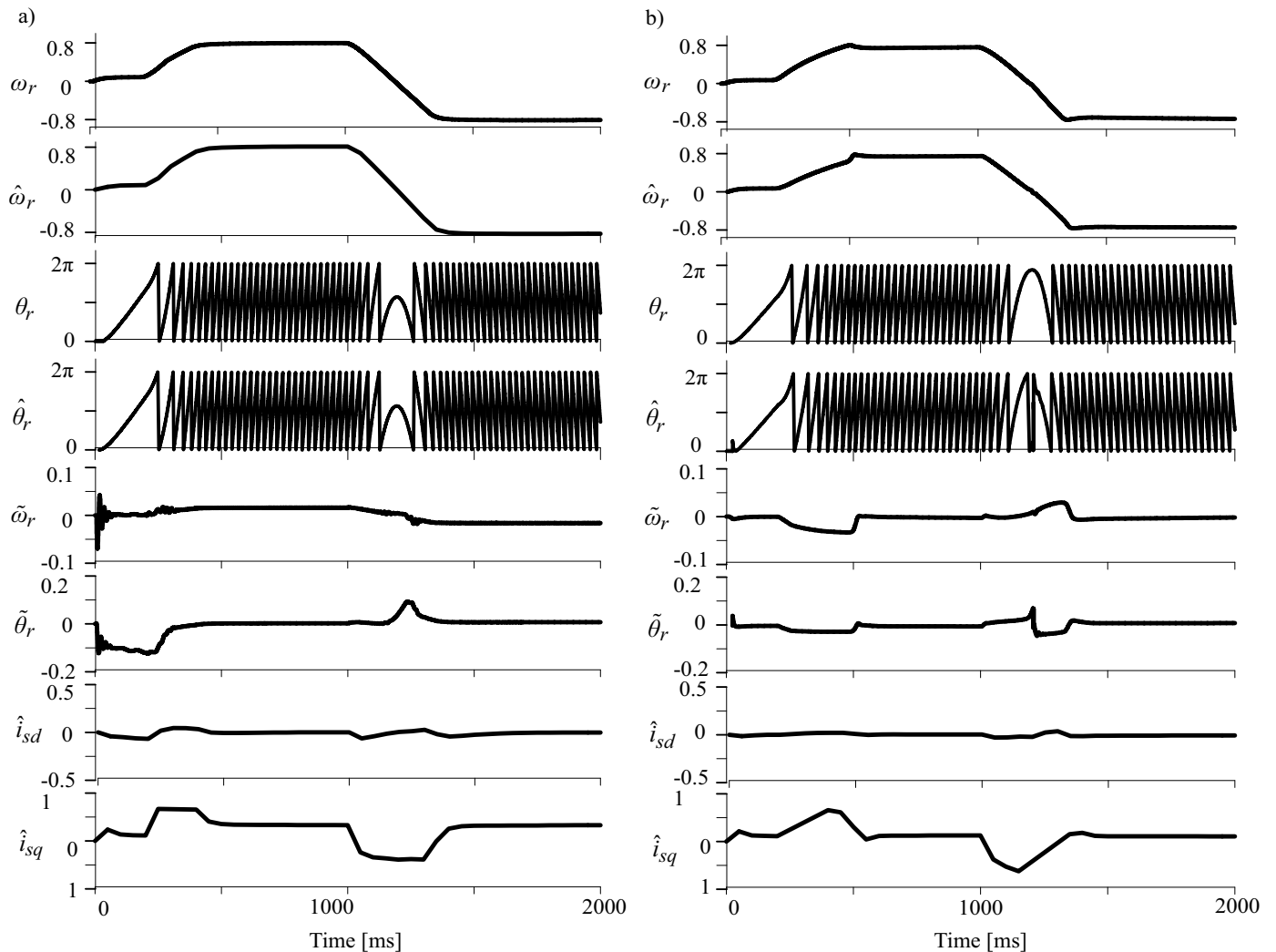


**Fig. 5.** Simulation results of observer structure for three-phase IPMSM drive: a) adaptive-based; b) non-adaptive-based

6

*Bull. Pol. Acad. Sci. Tech. Sci.*, vol. 72, no. 4, p. e150327, 2024

## 5. EXPERIMENTAL RESULTS AND DISCUSSION

The experimental test was conducted on a 3.5 kW IPMSM drive system. Slot harmonics and non-sinusoidal distribution are present in IPMSM, which can be seen in Fig. 2. The voltage source converter supplies the voltage to the IPMSM drive. The parameters of the IPMSM drives are specified in Table 1. The control scheme was implemented in an interface with a DSP Sharc ADSP21363 floating-point signal processor and Altera Cyclone 2 FPGA. The switching frequency of the transistor was 3.3 kHz, and the sampling time was 150 µs (6.6 kHz). The vector control scheme is shown in Fig. 4. The computation time of the control system is 49 µs without implementing code optimization.

### Table 1
Parameters of the IPMSM

| Parameter name | Symbol | Value | Unit |
|---|---|---|---|
| Stator resistance | $R_{sN}$ | 0.035 | p.u. |
| d-axis inductances | $L_{dN}$ | 0.28 | p.u. |
| q-axis inductances | $L_{qN}$ | 0.82 | p.u. |
| Permanent magnet flux linkage | $\psi_f$ | 0.89 | p.u. |
| Nominal value of electromagnetic torque | $TeN$ | 0.81 | p.u. |
| Nominal power | $Pn$ | 3.5 | kW |
| Nominal stator current (star (y)) | $In$ | 7.5 | A |
| Nominal stator voltage (star (y)) | $Un$ | 285 | V |
| Nominal rotor speed | $n$ | 1500 | rpm |
| Nominal frequency | $f$ | 50 | Hz |
| Reference voltage | $Ub = Un$ | 285 | V |
| Reference current | $Ib = In\sqrt{3}$ | 12.97 | A |

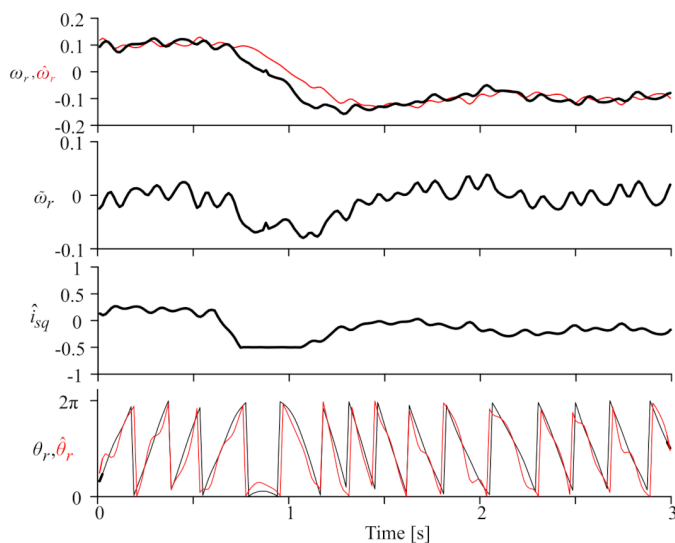In Fig. 6 reversal of IPMSM drive is shown from 0.1 to −0.1 using adaptive observer structure. The observer structure is based on a sinusoidal machine model. Due to machine asymmetry shown in Fig. 2, small oscillation can be seen in the observer results especially during low-speed operation of the IPMSM drive. However, the estimation of speed and position accurately follows the measured parameters of speed and position. Estimated current and speed errors are also shown.

In Fig. 7 a non-adaptive EEMF-based observer structure is implemented for the IPMSM drive. In Fig. 7a, the IPMSM drive is reversed from 0.1 to −0.1. At zero crossing, the estimated speed and position become completely unobservable. In Fig. 7b, IPMSM is reversed from −0.1 to 0.1. However, the observer speed struggles to reverse the IPMSM drive but suffers heavily due to machine disturbances. Overall, in both cases, as shown in Figs. 7a and 7b do not provide satisfactory results of the IPMSM drive at low speed. Other estimated parameters are also given in Fig. 7.
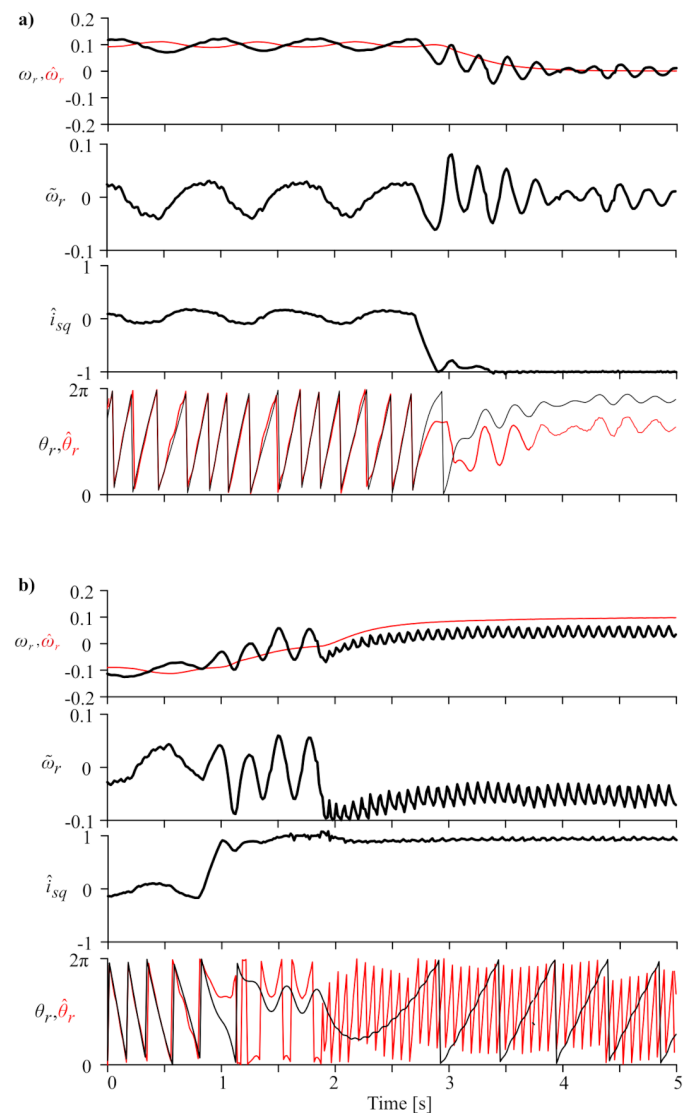


**Fig. 7.** IPMSM is reversing using non-adaptive EEMF observer: a) 0.1 to −0.1; b) −0.1 to 0.1



**Fig. 6.** IPMSM is reversing from 0.1 to −0.1 using adaptive observer

Results of the IPMSM drive starting up from 0.1 to 1.0 using adaptive and non-adaptive EEMF-based observer structures are visible in Figs. 8a and 8b. Error during the transient state is

*Bull. Pol. Acad. Sci. Tech. Sci.*, vol. 72, no. 4, p. e150327, 2024

7

less in the adaptive observer structure. The observer structure follows the measured value of speed and position, respectively. It can also be seen that the effect of considered disturbances does not impact observer estimation at medium and high-speed ranges as compared to low-speed ranges.
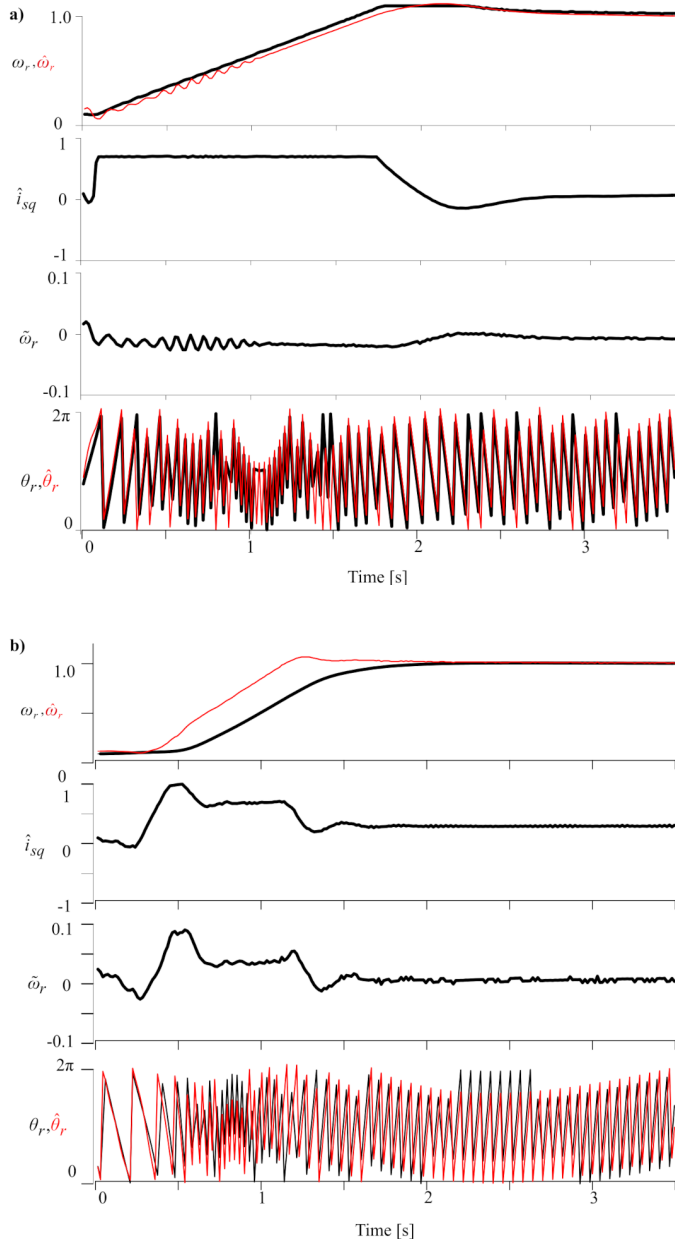
EEMF-based observer structure. Comparative analysis between the two observer structures at a wide speed range is provided in Table 2.



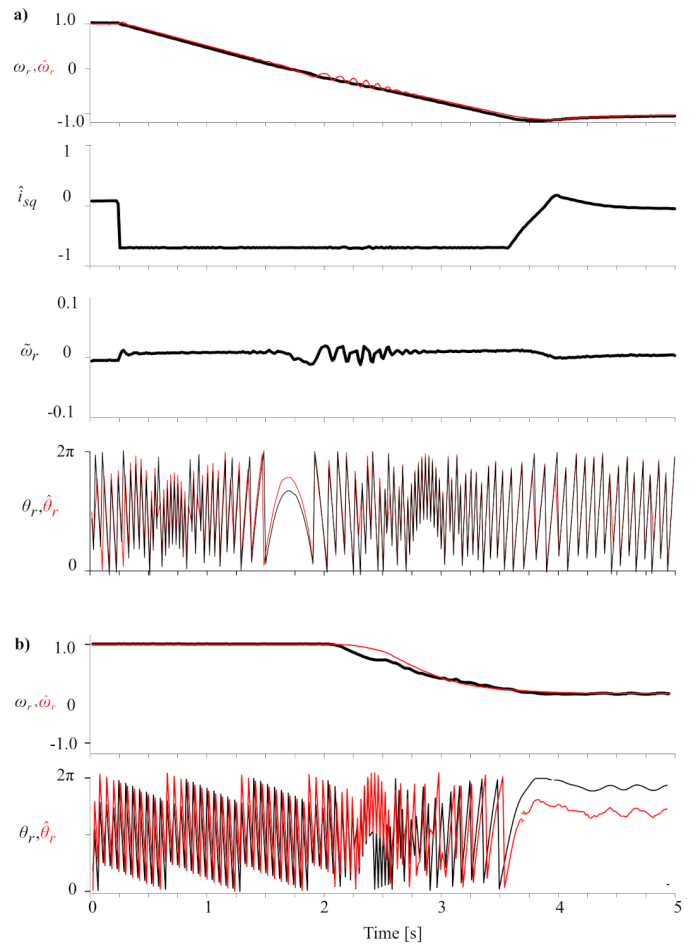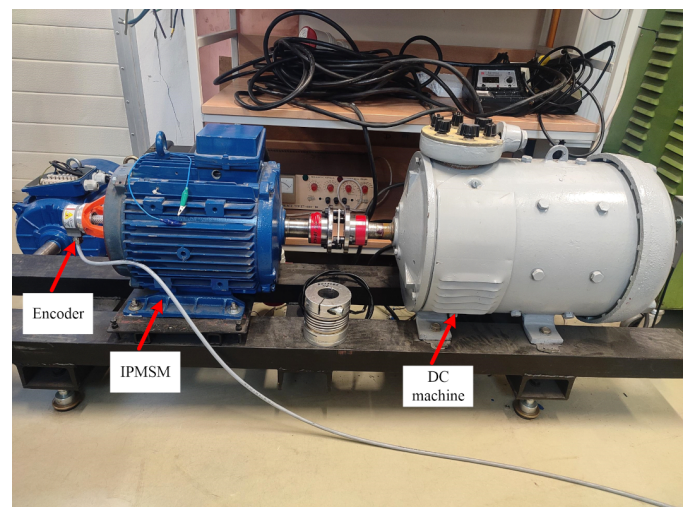**Fig. 8.** IPMSM starts up from 0.1 to 1.0: a) adaptive observer, b) non-adaptive EEMF observer



**Fig. 9.** IPMSM reverses up from 1.0 to −1.0: a) adaptive observer; b) non-adaptive EEMF observer

IPMSM drive reversal from 1.0 to −1.0 is shown in Fig. 9. Adaptive estimation successfully crosses the zero-speed range, while EEMF-based non-adaptive estimation struggles during zero speed and becomes unobservable. The primary reason behind this issue is that at zero speed, EMF is very small, which is not enough for the observer structure to estimate the speed. Considering the results of IPMSM at a wide speed range, the adaptive observer structure is more robust than the non-adaptive



**Fig. 10.** Photo of the experimental stand with the IPMSM clutched to the DC machine

8

*Bull. Pol. Acad. Sci. Tech. Sci.*, vol. 72, no. 4, p. e150327, 2024

**Table 2**
Comparison of the observer structures at a wide speed range

| Speed range | Adaptive observer structure | Non-adaptive EEMF based structure |
|---|---|---|
| Zero crossing | Stable | Not-stable |
| Low speed | Stable | Stable |
| Medium speed | Stable | Stable |
| High speed | Stable | Not-stable |

## 6. CONCLUSIONS

This paper presents an adaptive rotor flux-based observer structure and non-adaptive EEMF-based observer structure in ($\alpha$-$\beta$) reference frame to estimate speed and position. With the defined errors in the observer structure, adaptive law is employed to estimate speed in the adaptive observer structure. In the case of non-adaptive EEMF, observer structure speed is calculated using the dependencies of EMF and flux components. Considering the obtained estimation errors, stabilizing functions are prepared for the observer structure. The additional stabilizing functions increase the robustness of the observer structure. Stabilizing function formed using the Lyapunov stability theorem. The problem of non-sinusoidal distribution of EMF and slot harmonics is visible at a lower speed range. Adaptive observer structure works quite well compared to non-adaptive EEMF-based observer structure during zero and low-speed operation. No signal injection is required to estimate speed and position at low speed. Simulation and experimental results confirm the working of observer structures presented in this article.

## REFERENCES

[1] G. Wang, M. Valla, and J. Solsona, "Position sensorless permanent magnet synchronous machine drives – A review," *IEEE Trans. Ind. Electron.*, vol. 67, no. 7, pp. 5830–5842, Jul. 2020, doi: 10.1109/TIE.2019.2955409.

[2] C. Ogbuka, C. Nwosu, and M. Agu, "Dynamic and steady state performance comparison of line-start permanent magnet synchronous motors with interior and surface rotor magnets," *Arch. Electr. Eng.*, vol. 65, no. 1, pp. 105–116, Mar. 2016, doi: 10.1515/aee-2016-0008.

[3] A. Młot, M. Korkosz, A. Lechowicz, J. Podhajecki, and S. Rawicki, "Electromagnetic analysis, efficiency map and thermal analysis of an 80-kW IPM motor with distributed and concentrated winding for electric vehicle applications," *Arch. Electr. Eng.*, vol. 71, no. 4, pp. 981–1002, 2022, doi: 10.24425/aee.2022.142120.

[4] A. Mlot, M. Kowol, J. Kolodziej, A. Lechowicz, and P. Skrobotowicz, "Analysis of IPM motor parameters in an 80-kW traction motor," *Arch. Electr. Eng.*, vol. 69, no. 2, pp. 467–481, 2020, doi: 10.24425/aee.2020.133038.

[5] S. Brock and T. Pajchrowski, "Sensorless and energy-efficient PMSM drive for fan application," *Arch. Electr. Eng.*, Jun. 2013, pp. 217–225. doi: 10.2478/aee-2013-0017.

[6] H. Qiu, Y. Zhang, C. Yang, and R. Yi, "Influence of the number of turns on the performance of permanent magnet synchronous motor," *Bull. Pol. Acad. Sci. Tech. Sci.*, vol. 68, no. 3, pp. 429–436, Jun. 2020, doi: 10.24425/bpasts.2020.133375.

[7] R. Ryndzionek, K. Blecharz, F. Kutt, M. Michna, and G. Kostro, "Fault-Tolerant Performance of the Novel Five-Phase Doubly-Fed Induction Generator," *IEEE Access*, vol. 10, pp. 59350–59358, 2022, doi: 10.1109/ACCESS.2022.3179815.

[8] Y. Li, H. Hu, and P. Shi, "A Review of Position Sensorless Compound Control for PMSM Drives," *World Electr. Veh. J.*, vol. 14, no. 2, p. 34, 2023. doi: 10.3390/wevj14020034.

[9] M. Tang, C. Wang, and Y. Luo, "Predictive current control for permanent magnet synchronous motor based on internal model control observer," *Arch. Electr. Eng.*, vol. 71, no. 2, pp. 343–362, 2022, doi: 10.24425/aee.2022.140715.

[10] S. Navaneethan, S. Kanthalakshmi, and S. Aandrew Baggio, "Lyapunov stability based sliding mode observer for sensorless control of permanent magnet synchronous motor," *Bull. Pol. Acad. Sci. Tech. Sci.*, vol. 70, no. 2, p. e140353, 2022, doi: 10.24425/bpasts.2022.140353.

[11] M. Morawiec, A. Lewicki, and C. Odeh, "Rotor-Flux Vector based Observer of Interior Permanent Synchronous Machine," *IEEE Trans. Ind. Electron.*, vol. 71, no.2, pp. 1399–1409, 2024, doi: 10.1109/TIE.2023.3250851.

[12] J. Choi, K. Nam, A.A. Bobtsov, and R. Ortega, "Sensorless Control of IPMSM Based on Regression Model," *IEEE Trans. Power Electron.*, vol. 34, no. 9, pp. 9191–9201, Sep. 2019, doi: 10.1109/TPEL.2018.2883303.

[13] M.P. Kazmierkowski and H. Tunia, *Automatic Control of Converter-Fed Drives*. Amsterdam, London, New York, Tokyo, Warsaw: Elsevier, 1994, pp. 37–68.

[14] A. T. Woldegiorgis, X. Ge, H. Wang, and M. Hassan, "A New Frequency Adaptive Second-Order Disturbance Observer for Sensorless Vector Control of Interior Permanent Magnet Synchronous Motor," *IEEE Trans. Ind. Electron.*, vol. 68, no. 12, pp. 11847–11857, Dec. 2021, doi: 10.1109/TIE.2020.3047065.

[15] T. Zhang, Z. Xu, J. Li, H. Zhang, and C. Gerada, "A third-order super-twisting extended state observer for dynamic performance enhancement of sensorless IPMSM drives," *IEEE Trans. Ind. Electron.*, vol. 67, no. 7, pp. 5948–5958, Jul. 2020, doi: 10.1109/TIE.2019.2959498.

[16] Z. Xu, T. Zhang, Y. Bao, H. Zhang, and C. Gerada, "A nonlinear extended state observer for rotor position and speed estimation for sensorless IPMSM Drives," *IEEE Trans. Power Electron.*, vol. 35, no. 1, pp. 733–743, Jan. 2020, doi: 10.1109/TPEL.2019.2914119.

[17] A. T. Woldegiorgis, X. Ge, S. Li, and M. Hassan, "Extended Sliding Mode Disturbance Observer-Based Sensorless Control of IPMSM for Medium and High-Speed Range Considering Railway Application," *IEEE Access*, vol. 7, pp. 175302–175312, 2019, doi: 10.1109/ACCESS.2019.2957274.

*Bull. Pol. Acad. Sci. Tech. Sci.*, vol. 72, no. 4, p. e150327, 2024

9

D. Vyas, M. Morawiec, and D. Wachowiak

[18] D. Xiao, S. Nalakath, Y. Sun, J. Wiseman, and A. Emadi, "Complex-coefficient adaptive disturbance observer for position estimation of IPMSMs with robustness to DC Errors," *IEEE Trans. Ind. Electron.*, vol. 67, no. 7, pp. 5924–5935, Jul. 2020, doi: 10.1109/TIE.2019.2941157.

[19] Y. Zhang, Z. Yin, C. Bai, G. Wang, and J. Liu, "A Rotor Position and Speed Estimation Method Using an Improved Linear Extended State Observer for IPMSM Sensorless Drives," *IEEE Trans. Power Electron.*, vol. 36, no. 12, pp. 14062–14073, Dec. 2021, doi: 10.1109/TPEL.2021.3085126.

[20] I. Boldea, M.C. Paicu, and G.D. Andreescu, "Active flux concept for motion-sensorless unified AC drives," *IEEE Trans. Power Electron.*, vol. 23, no. 5, pp. 2612–2618, 2008, doi: 10.1109/TPEL.2008.2002394.

[21] I. Boldea, M.C. Paicu, G.D. Andreescu, and F. Blaabjerg, "'Active Flux' DTFC-SVM sensorless control of IPMSM," *IEEE Trans. Energy Convers.*, vol. 24, no. 2, pp. 314–322, 2009, doi: 10.1109/TEC.2009.2016137.

[22] K. Urbanski, "Determining the observer parameters for back EMF estimation for selected types of electrical motors," *Bull. Pol. Acad. Sci. Tech. Sci.*, vol. 65, no. 4, pp. 439–447, Aug. 2017, doi: 10.1515/bpasts-2017-0049.

[23] J. Yang, M. Dou, and D. Zhao, "Iterative sliding mode observer for sensorless control of five-phase permanent magnet synchronous motor," *Bull. Pol. Acad. Sci. Tech. Sci.*, vol. 65, no. 6, pp. 845–857, 2017, doi: 10.1515/bpasts-2017-0092.

[24] Y. Zhao, W. Qiao, and L. Wu, "Improved Rotor Position and Speed Estimators for Sensorless Control of Interior Permanent-Magnet Synchronous Machines," *IEEE J. Emerg. Sel. Top Power Electron.*, vol. 2, no. 3, pp. 627–639, Jan. 2014, doi: 10.1109/jestpe.2014.2298433.

[25] A. Glumineau, J. De, and L. Morales, *Sensorless AC Electric Motor Control Robust Advanced Design Techniques and Applications – Advances in Industrial Control*. Springer Cham, 2015, doi: 10.1007/978-3-319-14586-0.

[26] R. Krishnan, *Permanent magnet synchronous and brushless DC motor drives*. CRC Press/Taylor & Francis, 2010.

[27] G. Wang, G. Zhang, and D. Xu, *Position Sensorless Control Techniques for Permanent Magnet Synchronous Machine Drives*. Springer, 2020.

[28] M. Morawiec and K. Blecharz, "Non-adaptive Speed and Position Estimation of Doubly-Fed Induction Generator in Grid-Connected Operations," *IEEE Trans. Ind. Electron.*, vol. 71, no.2, pp. 3617–3627, 2024, doi: 10.1109/TIE.2023.3279548.

10

*Bull. Pol. Acad. Sci. Tech. Sci.*, vol. 72, no. 4, p. e150327, 2024